Quantum breathing mode of interacting particles in a one-dimensional harmonic trap

Jan Willem Abraham,* Karsten Balzer, David Hochstuhl, and Michael Bonitz
Institut für Theoretische Physik und Astrophysik, Christian-Albrechts-Universität zu Kiel, Leibnizstraße 15, D-24098 Kiel, Germany
(Received 12 March 2012; revised manuscript received 28 July 2012; published 10 September 2012)

Extending our previous work, we explore the breathing mode—the (uniform) radial expansion and contraction of a spatially confined system. We study the breathing mode across the transition from weak to moderate couplings and confirm that its frequency is not independent of the pair interaction strength (coupling parameter). We present the results of time-dependent Hartree-Fock simulations for 2 to 20 fermions with Coulomb interaction and show that the breathing frequency has a minimum for a small particle number. We validate the accuracy of our results, comparing them to exact configuration interaction results for up to eight particles.

DOI: 10.1103/PhysRevB.86.125112 PACS number(s): 73.22.Lp, 03.75.Kk, 03.75.Ss, 05.30.−d

I. INTRODUCTION

Harmonically confined few-particle quantum systems and especially their time-dependent properties are an important subject of experimental and theoretical research activities. For example, correlated electrons in metal clusters[1] or quantum dots[2–4] and ultracold Bose and Fermi gases in traps or optical lattices[5,6] have been investigated in recent years. Particularly, Bose-Einstein condensation in low dimensions[7] and nonideality (interaction) effects,[8–11] including superfluidity and crystallization,[12,13] lately raised attention.

The major diagnostic of the properties of finite trapped systems is the analysis of their collective excitations or normal modes. This spectrum is of the same importance as atomic or molecular spectra of conventional materials. Among the collective excitations the breathing mode (BM) attracts special interest, as it is easily excited experimentally[9] and very accurately measurable. At the same time, it was shown[14] that the frequency of the breathing motion—the (uniform) radial expansion and contraction of the whole system—contains detailed information on a variety of system properties. The BM of a nonideal quantum system is characterized by two frequencies. In our previous work,[14] we have shown for a two-particle system that one of those frequencies changes with the system dimensionality, the particle spin and the strength of the pair interaction. These results were extended[15] to four and six particles and to different inverse power law interaction potentials $w(r) \propto r^{-d}$ with $d = 1,2,3$.

Having concentrated, in our previous works, on the transition from weak to strong coupling, here we investigate the *influence of the particle number on the breathing frequency* for various fixed coupling strengths. For that purpose, we perform time-dependent Hartree-Fock (TDHF) simulations for up to $N = 20$ particles in a quantum statistical description. After a short theoretical introduction, we show these new results for finite systems and compare the frequencies for small particle numbers to those from first-principles configuration interaction simulations and from the solution of the time-dependent Schrödinger equation. This comparison shows that the TDHF data reproduce the correct trends for the breathing frequency and can be used to study the N dependence also for larger systems where first-principles results are not available.

As an interesting result we report that the breathing frequency changes nonmonotonically with the particle number. It reaches a minimun around $N = 5,\ldots,6$ for small and moderate values of the coupling parameter. The existence of this minimum is unexpected, and we conclude the paper by discussing the physical origin of this effect: the existence of a maximum of nonideality effects around these N values at a fixed value of the coupling parameter in the trap.

II. THEORY

A. Time-dependent Schrödinger equation

We briefly recall the theoretical background of the BM.[14,15] Generally, a system of N interacting particles with coordinates $\mathbf{r} \equiv (\mathbf{r}_1,\ldots,\mathbf{r}_N)$ can be described by the Hamiltonian

$$H_0(\mathbf{r}) = \sum_{i=1}^{N} h(\mathbf{r}_i) + \sum_{i<j}^{N} w(|\mathbf{r}_i - \mathbf{r}_j|)\,, \tag{1}$$

where

$$h_i = t_i + v(\mathbf{r}_i) \tag{2}$$

is the single-particle Hamiltonian and $w(|\mathbf{r}_i - \mathbf{r}_j|)$ is a binary interaction potential. The external single-particle potential $v(\mathbf{r}_i)$ is chosen to be harmonic,

$$v(\mathbf{r}_i) = \tfrac{1}{2} m\Omega^2 \mathbf{r}_i^2\,. \tag{3}$$

v serves as a trapping potential with the trapping frequency Ω. In the following, we concentrate on Coulomb-interacting particles with equal masses m and equal charges e, e.g., electrons or ions. Thus the interaction potential has the form

$$w(|\mathbf{r}_i - \mathbf{r}_j|) = \frac{a}{|\mathbf{r}_i - \mathbf{r}_j|}, \tag{4}$$

with $a \equiv e^2/(4\pi\varepsilon_0)$. Finally, the N-particle time-dependent Schrödinger equation (TDSE) reads

$$\mathrm{i}\hbar\frac{\partial}{\partial t}\Psi(\mathbf{r},t) = \left[\sum_{i=1}^{N}\left(-\frac{\hbar^2}{2m}\frac{\partial^2}{\partial \mathbf{r}_i^2} + \frac{1}{2}m\Omega^2\mathbf{r}_i^2\right) + \sum_{i<j}^{N}\frac{a}{|\mathbf{r}_i - \mathbf{r}_j|}\right]\Psi(\mathbf{r},t)\,. \tag{5}$$

For convenience, we introduce the scaled quantities $\tilde{\mathbf{r}}_i = \mathbf{r}_i/l_0$ and $\tilde{t} = \Omega t$, so that after omitting the tilde symbol, the TDSE

can be written in the dimensionless form

$$i\frac{\partial}{\partial t}\Psi(\mathbf{r},t) = \left[\frac{1}{2}\sum_{i=1}^{N}\left(-\frac{\partial^2}{\partial \mathbf{r}_i^2}+\mathbf{r}_i^2\right) + \lambda\sum_{i<j}^{N}\frac{1}{|\mathbf{r}_i-\mathbf{r}_j|}\right]\Psi(\mathbf{r},t)\,, \tag{6}$$

where $l_0 = [\hbar/(m\Omega)]^{1/2}$ is the well-known oscillator length and

$$\lambda = \frac{mal_0}{\hbar^2} \tag{7}$$

is the *Coulomb coupling parameter for the harmonic trap*. Due to the rescaling, there will only be dimensionless quantities throughout this work. For example, lengths, times and energies are given in units of l_0, Ω^{-1}, and $\hbar\Omega$, respectively. The meaning of λ can be interpretated as follows. Defining the scale of the potential energy as

$$E_0 = \tfrac{1}{2}m\Omega^2 l_0^2 \tag{8}$$

and the mean interaction energy as

$$E_C = \frac{a}{2l_0}\,, \tag{9}$$

one finds

$$\lambda = \frac{E_C}{E_0}\,. \tag{10}$$

Hence λ can be understood as the ratio of the interaction energy and the confinement energy. The influence of the value of λ is described later in Sec. II C.

The actual excitation of the breathing mode is realized by a fast switch of the trapping potential. For a short period of time $t_{\rm exc}$ the trap frequency is decreased from Ω to $\tilde{\Omega}$. Characterizing the excitation strength by a small parameter η, the time-dependent Hamiltonian thus takes the form

$$H(t) = \sum_{i=1}^{N} h_i + \eta\left[\theta(t_0-t)+\theta(t-t_{\rm exc})\right]v(\mathbf{r}_i) + \sum_{i<j}^{N} w(|\mathbf{r}_i-\mathbf{r}_j|)\,. \tag{11}$$

The additional term contains the operator for the monopole excitation ($\sum_i \mathbf{r}_i^2$). The excitation drives the particles out of their initial state. When the potential is restored, the time-dependent expectation value of some quantities start to oscillate. While a classical treatment of the breathing mode allows for the observation of oscillating particle coordinates $\mathbf{r}_i(t)$, the expectation value of the quantity $\mathbf{r} = \sum_i \mathbf{r}_i$ is always zero. The single-particle potential energy $E_{\rm pot} = \sum_i v(\mathbf{r}_i)$, however, has a nonvanishing expectation value, as it is proportional to $\mathbf{r}_i^2$. Its oscillation is dominated by a beating of two frequencies,[14] which will be denoted ω_r and ω_R from now on. Both a typical time series of the potential energy and the rapid excitation process are demonstrated in Fig. 1. In the next sections, we want to point out some analytically accessible properties of the frequencies and their relations to the coupling parameter λ.

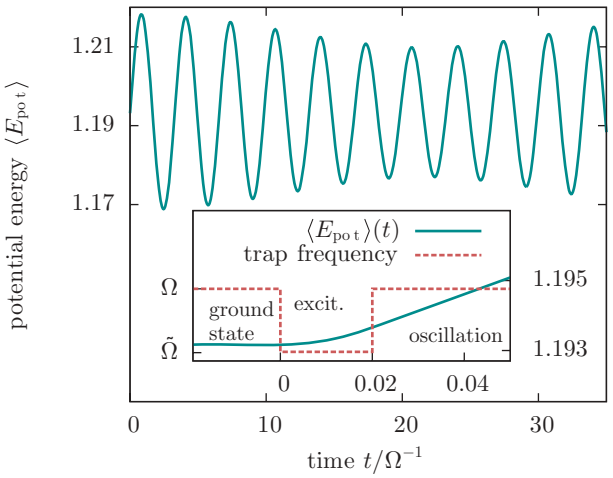

FIG. 1. (Color online) Exemplary time series ($N = 2$, $\lambda = 1$) of the potential energy $\langle E_{\rm pot}\rangle$. The waveform shows a superposition of two harmonic oscillations with the dominating frequencies ω_r and ω_R. The inset demonstrates the excitation of the breathing mode, involving a decrease of the trap frequency from Ω to $\tilde{\Omega}$ (note the very short time interval $t_{\rm exc} = 0.02$).

B. Separation of center-of-mass motion

In the general quantum case, the system of two particles, for arbitrary λ, possesses a universal breathing mode whose frequency has the value $\omega_R = 2$. This is a remarkable property as this mode does not show up at all in a classical treatment. In the following, we generalize the derivation presented in our previous work[14] for $N = 2$ and show that this frequency is independent of the coupling strength, the system dimensionality, and the particle number.

The basic idea for the solution of Eq. (6) is the introduction of center-of-mass and relative coordinates, which allows to split the Hamiltonian in two independent parts. The center-of-mass coordinate is given by

$$\mathbf{R} \equiv \frac{1}{N}\sum_{i=1}^{N}\mathbf{r}_i\,, \tag{12}$$

and the set of relative coordinates is

$$\mathbf{x} \equiv (\mathbf{x}_1, \mathbf{x}_2, \ldots, \mathbf{x}_{N-1})\,, \tag{13}$$

with the definition $\mathbf{x}_i \equiv \mathbf{r}_{i,i+1} \equiv \mathbf{r}_{i+1} - \mathbf{r}_i$. Thus $\Psi(\mathbf{r},t)$ in Eq. (6) is replaced by $\Psi(\mathbf{R},\mathbf{x},t)$. Now the transformation is shown for each term in Eq. (6), starting with

$$-\frac{1}{2}\sum_{i=1}^{N}\frac{\partial^2}{\partial \mathbf{r}_i^2} = -\frac{1}{2}\left(\sum_{i=1}^{N}\frac{\partial^2}{\partial \mathbf{R}^2}\frac{1}{N^2} + 2\sum_{i=1}^{N-1}\frac{\partial^2}{\partial \mathbf{x}_i^2}\right) = -\frac{1}{2N}\frac{\partial^2}{\partial \mathbf{R}^2} - \sum_{i=1}^{N-1}\frac{\partial^2}{\partial \mathbf{x}_i^2}\,. \tag{14}$$

For the second term, we obtain

$$\frac{1}{2}\sum_{i=1}^{N}\mathbf{r}_i^2 = \frac{1}{2}N\mathbf{R}^2 + \frac{1}{4N}\sum_{i=1}^{N}\sum_{k=1}^{N}\mathbf{r}_{ik}^2\,, \tag{15}$$

where $\mathbf{r}_{ik}^2$ still has to be expressed in relative coordinates $\mathbf{x}$. This can be done as follows:

$$\mathbf{r}_{ik} = \begin{cases} \sum_{l=i}^{k-1} \mathbf{x}_l & \text{for } i < k, \\ \sum_{l=k}^{i-1} \mathbf{x}_l & \text{for } i > k, \\ 0 & \text{for } i = k. \end{cases} \tag{16}$$

Finally, the third term takes the form

$$\lambda \sum_{i<j}^{N} \frac{1}{|\mathbf{r}_i - \mathbf{r}_j|} = \lambda \sum_{i<j}^{N} \frac{1}{\left|\sum_{l=i}^{j-1} \mathbf{x}_l\right|} . \tag{17}$$

As a result, the Hamiltonian can be split in two independent contributions:

$$H_{\mathbf{R}} = -\frac{1}{2N}\frac{\partial^2}{\partial \mathbf{R}^2} + \frac{1}{2} N \mathbf{R}^2 \tag{18}$$

and

$$H_{\mathbf{x}} = -\sum_{i=1}^{N-1} \frac{\partial^2}{\partial \mathbf{x}_i^2} + \frac{1}{4N} \sum_{i=1}^{N} \sum_{k=1}^{N} \mathbf{r}_{ik}^2 + \lambda \sum_{i<j}^{N} \frac{1}{\left|\sum_{l=i}^{j-1} \mathbf{x}_l\right|}. \tag{19}$$

Hence the TDSE takes the form

$$\mathrm{i}\frac{\partial}{\partial t}\Psi(\mathbf{R},\mathbf{x},t) = (H_{\mathbf{R}} + H_{\mathbf{x}})\,\Psi(\mathbf{R},\mathbf{x},t) . \tag{20}$$

Separating the coordinates in the factorized wave function

$$\Psi(\mathbf{R},\mathbf{x},t) = \phi(\mathbf{R},t)\,\varphi(\mathbf{x},t) \tag{21}$$

yields the independent problems

$$\mathrm{i}\frac{\partial}{\partial t}\phi(\mathbf{R},t) = H_{\mathbf{R}}\phi(\mathbf{R},t) \tag{22}$$

and

$$\mathrm{i}\frac{\partial}{\partial t}\varphi(\mathbf{x},t) = H_{\mathbf{x}}\varphi(\mathbf{x},t) . \tag{23}$$

The center-of-mass problem can be transformed to the standard oscillator form

$$\mathrm{i}\frac{\partial}{\partial t}\phi(\tilde{\mathbf{R}},t) = \left(-\frac{1}{2}\frac{\partial^2}{\partial \tilde{\mathbf{R}}^2} + \frac{1}{2}\tilde{\mathbf{R}}^2\right)\phi(\tilde{\mathbf{R}},t) , \tag{24}$$

where the rescaling $\tilde{\mathbf{R}} = \sqrt{N}\mathbf{R}$ has been used. Now consider an initial state, which can be expressed by

$$\phi(\tilde{\mathbf{R}},t=0) = \sum_n c_n \phi_n(\tilde{\mathbf{R}}) , \tag{25}$$

where ϕ_n is a solution of

$$\left(-\frac{1}{2}\frac{\partial^2}{\partial \tilde{\mathbf{R}}^2} + \frac{1}{2}\tilde{\mathbf{R}}^2\right)\phi_n(\tilde{\mathbf{R}}) = E_n\phi_n(\tilde{\mathbf{R}}) . \tag{26}$$

The associated energy eigenvalues are well known: $E_n = n + d/2$ for all $n \in \{0,1,2,\dots\}$, and the time evolution of the state in Eq. (25) is given by

$$\phi(\tilde{\mathbf{R}},t) = \sum_n c_n \phi_n(\tilde{\mathbf{R}}) \mathrm{e}^{-\mathrm{i}E_n t} . \tag{27}$$

The breathing mode manifests itself in the dynamics of the quantity $\mathbf{r}^2 = \sum_{i=1}^{N} \mathbf{r}_i^2$. Using center-of-mass and relative coordinates, this quantity can be expressed according to Eq. (15). For the first term in Eq. (15), a breathing frequency can be obtained by determining the expectation value

$$\langle \mathbf{R}^2 \rangle(t) = N^{-1/2} \langle \tilde{\mathbf{R}}^2 \rangle(t) . \tag{28}$$

The result for this expression is

$$\begin{aligned} \langle \tilde{\mathbf{R}}^2 \rangle(t) &= \int \mathrm{d}\tilde{\mathbf{R}}\,\mathrm{d}\mathbf{x}\,\Psi^*(\tilde{\mathbf{R}},\mathbf{x},t)\tilde{\mathbf{R}}^2\Psi(\tilde{\mathbf{R}},\mathbf{x},t) \\ &= \sum_{i,j} c_i^* c_j \mathrm{e}^{-\mathrm{i}(j-i)t} (\tilde{\mathbf{R}}^2)_{ij} , \end{aligned} \tag{29}$$

with

$$(\tilde{\mathbf{R}}^2)_{ij} = \int \mathrm{d}\tilde{\mathbf{R}}\,\phi_i^*(\tilde{\mathbf{R}})\tilde{\mathbf{R}}^2\phi_j(\tilde{\mathbf{R}}) . \tag{30}$$

It can be shown with a reduction to the matrix elements of a one-dimensional harmonic oscillator that only the cases $i = j$ and $i = j \pm 2$ contribute to the last summation in Eq. (29) (the case $i = j$ does not correspond to an oscillation). The only frequency appearing in the oscillation is thus given by $\omega_R = 2$. As the coupling parameter λ does not appear in the center-of-mass problem, the center-of-mass mode with frequency $\omega_R = 2$ is present for all couplings. In summary, we have shown that the frequency ω_R is universal, but its amplitude tends to vanish for large particle numbers since it is proportional to $N^{-1/2}$.

C. Influence of coupling parameter and limiting cases

As we have seen in the last section, the introduction of relative and center-of-mass coordinates has led to a separation ansatz. The center-of-mass Hamiltonian $H_{\mathbf{R}}$ yields a breathing frequency $\omega_R = 2$. It has already been mentioned that the breathing motion also exhibits another frequency ω_r. The properties of this frequency are an interesting subject of numerical analysis. Only in two limiting cases, it is known from analytical calculations that the values of ω_r are universal. In the pure quantum limit, (ideal system, $\lambda = 0$), the particles are completely uncorrelated. As the interaction term in the Hamiltonian is missing, a two-fold degenerate frequency $\omega_r = \omega_R = 2$ occurs. On the contrary, in the strongly coupled classical limit, $\lambda \to \infty$, the frequency ω_r has the value $\sqrt{3}$.[16–18] In both cases, the frequency does not depend on the particle number or the dimensionality of the system. For arbitrary values of the coupling parameters, ω_r is expected to be in the interval $[\sqrt{3},2]$. To clarify the influence of the system parameters such as the coupling parameter λ and the particle number N on ω_r is one of the main goals of our investigation.

III. SIMULATION METHODS

While the solution of the time-dependent Schrödinger equation could only be performed for two particles, the frequencies for up to eight particles are still accessible through exact configuration interaction calculations. These results are used to support the accuracy of time-dependent Hartree-Fock calculations, which have been performed for even higher particle numbers (up to 20).

Due to the high computational effort, we restrict ourselves to the solution of a one-dimensional system. Nevertheless, such a system can be regarded as a basic theoretical model that requires a deepened understanding. In order to suppress

spin effects, only spin-polarized systems are investigated. At the beginning, the system is in the energetically lowest antisymmetric state.

Before presenting the numerical results in Sec. IV, we give a brief discussion of the employed methods. It shall already be mentioned here that, in order to avoid divergencies in the interaction potential, all methods use a regularized Coulomb potential $\lambda/|r_i - r_j + \kappa^2|$, where κ is a small finite cutoff parameter.

A. Time-dependent Schrödinger equation (TDSE)

In our previous work,[14] we determined $\omega_r(\lambda)$ for $N = 2$ in the whole range $\lambda = 0, \ldots, \infty$. These values are the basis for the comparison with other methods. Our TDSE results were obtained by solving the time-dependent Schrödinger equation with two different methods. On the one hand, a standard grid-based Crank-Nicolson scheme was used, and on the other hand, the wave function was expanded into a set of basis functions (oscillator eigenfunctions). The results confirm the values of the breathing frequencies in the limiting cases ($\lambda = 0$ and $\lambda = \infty$) and yield a continuous function $\omega_r(\lambda)$ for all other couplings in between.

B. Configuration interaction (CI)

Configuration interaction (CI) is another method for obtaining numerically exact solution of the TDSE. The basic idea of CI is to expand the wave function in a complete set of Slater determinants, which in turn are constructed with a complete single-particle basis. The ground-state wave function emerges from the eigenvalue problem

$$H_0|\Psi\rangle = E|\Psi\rangle \ . \tag{31}$$

In order to obtain the breathing frequencies, one can use the ground-state wave function and propagate it, according to the TDSE

$$\mathrm{i}\frac{\partial}{\partial t}|\Psi(t)\rangle = H(t)|\Psi(t)\rangle \ . \tag{32}$$

The frequencies can finally be extracted from the spectra of appropriate observables, e.g., $\langle E_{\mathrm{pot}}(t)\rangle$. This method is useful as it allows us to compare the spectra of an exact method with those from the time-dependent Hartree-Fock method (see the next section). However, there is another possibility to calculate the breathing frequencies. One can avoid a time propagation, if one assumes that the excitation is infinitely short. Hence the Hamiltonian can be written as

$$H(t) = H_0 + \eta\delta(t)\sum_{i=1}^{N} v(\mathbf{r}_i) \ , \tag{33}$$

where the time-independent part H_0 is that of Eq. (1). If H_0 is diagonalized by the eigenfunctions $|\Psi_n\rangle$ with eigenvalues E_n, the application of perturbation theory yields that the expectation value of an arbitrary observable can be calculated by

$$\langle A\rangle(t) = \sum_{i,j} c_i^* c_j \, e^{\mathrm{i}(E_i - E_j)t} \, \langle\Psi_i|A|\Psi_j\rangle \ , \tag{34}$$

where $c_{i,j}$ are time-independent coefficients. As a consequence of this relation, the oscillation of the expectation value is restricted to frequencies

$$\omega_{ij} \equiv |E_i - E_j| \ . \tag{35}$$

Instead of time-propagating the solution of the Schrödinger equation, we can use this result and extract the breathing frequencies from the eigenvalues of H_0 with relatively little computational effort.

Since in both of the above cases an exact diagonalization is involved, the CI method is only applicable for small particle numbers. All presented results were produced with a basis of oscillator functions. Especially for weak couplings, this basis set is well adjusted to the physical problem and the number of basis functions can be kept low. Just like the TDSE results the CI results can be used as a benchmark for the accuracy of the Hartree-Fock results.

C. Time-dependent Hartree-Fock (TDHF)

For larger particle numbers ($N \geqslant 8$), exact methods require a prohibitively large computational effort. Therefore, as a first step in treating large particle numbers, we describe the system in a reduced quantum statistical approach.[19] The key quantity of this description is the one-particle density operator F_1, which, in coordinate representation, is defined by the expectation value of the product of a creation and an annihilation operator:

$$F_1(x_1,x_2,t) = \langle\psi^\dagger(x_1,t)\psi(x_2,t)\rangle \ . \tag{36}$$

Using that definition, the expectation values $\langle O\rangle$ of spatially diagonal one-body operators $O = \sum_{i=1}^{N} o(x_i)$ can be calculated by

$$\langle O\rangle(t) = \int \mathrm{d}x \, o(x)n(x) \ , \tag{37}$$

where we introduced the density $n(x) \equiv F_1(x,x,t)$. The equation of motion for F_1 is the first equation of the BBGKY hierarchy,[19–23] which couples the one-particle density operator to the two-particle density operator. In order to decouple the hierarchy, we use the Hartree-Fock approximation, resulting in the following equation of motion for spin-polarized fermions:[19]

$$\begin{aligned}\left[\mathrm{i}\partial_t + \frac{1}{2}\left(\nabla^2_{\mathbf{r}'} - \nabla^2_{\mathbf{r}''}\right) - v(\mathbf{r}',t) + v(\mathbf{r}'',t)\right] F_1(\mathbf{r}',\mathbf{r}'',t) \\ = \int \mathrm{d}\bar{\mathbf{r}} \, \{w(|\mathbf{r}' - \bar{\mathbf{r}}|) - w(|\mathbf{r}'' - \bar{\mathbf{r}}|)\} \\ \times [F_1(\mathbf{r}',\mathbf{r}'',t)F_1(\bar{\mathbf{r}},\bar{\mathbf{r}},t) \ - F_1(\mathbf{r}',\bar{\mathbf{r}},t)F_1(\bar{\mathbf{r}},\mathbf{r}'',t)].\end{aligned} \tag{38}$$

In this equation, the two-particle density operator has been replaced by an approximate expression of the one-particle operators (see references and Appendix B for details). The problem is thus treated on the mean-field level, where the binary interactions are reduced to an effective single-particle potential: each particle is influenced by the field of all other particles. Furthermore, the excitation has been included into the operator $v(\mathbf{r},t)$.

The numerical implementation starts with a determination of the initial density matrix. For that purpose the Roothaan-Hall equations[24] are solved iteratively. In the elderly quantum chemistry literature, this method is commonly known as the self-consistent field method (SCF). For our calculations we

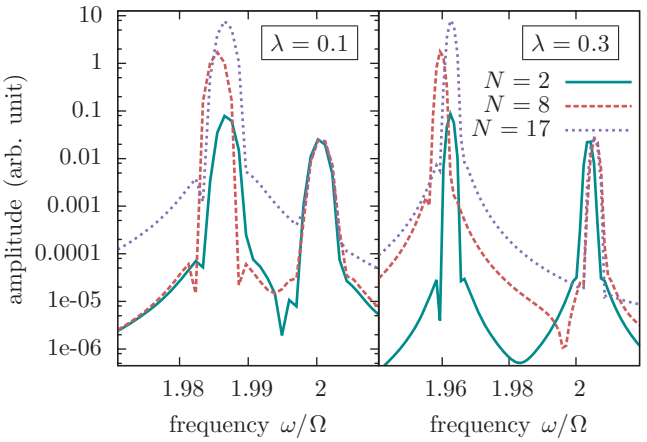

FIG. 2. (Color online) Monopole oscillation spectra for 2, 8, and 17 particles at two different coupling strengths λ. Each spectrum shows clearly dominating peaks for the frequencies ω_r (left) and ω_R (right). The data arise from propagations in the Hartree-Fock basis with $t_{\text{prop}} = 6000\ \Omega^{-1}$ and $\eta = -0.001$.

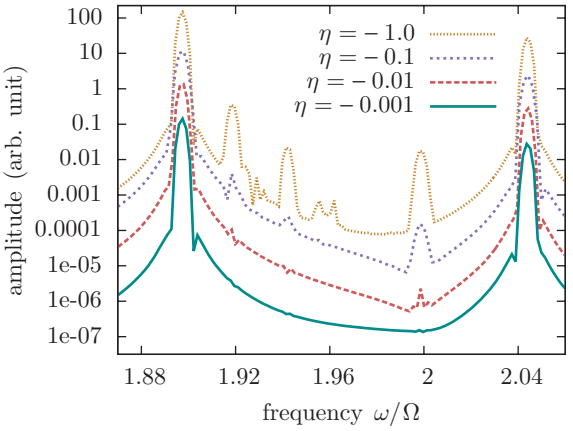

FIG. 3. (Color online) Influence of the excitation strength η on the Hartree-Fock spectrum around the breathing frequencies. The data correspond to the case $\lambda = 1$ and $N = 2$. Reducing the modulus of η to a very small value, one can always suppress additional peaks. While the leftmost and the rightmost peaks clearly scale down with η, the peak near $\omega = 2$ (which must not be confused with the center-of-mass peak) scales down with η^2.

use at least 400 FE-DVR (finite-element discrete variable representation[25,26]) basis functions. The next step is to integrate Eq. (38), i.e., propagate the density matrix in time. For this calculation, one can keep the FE-DVR basis, or equivalently, transform the equation of motion into the basis of Hartree-Fock orbitals. The latter approach is rather efficient because the number of necessary basis functions can be chosen in the order of N. The breathing frequencies are finally extracted from the spectra, which are obtained from the time series of the single-particle potential energy $\langle E_{\text{pot}} \rangle$.

IV. RESULTS

As mentioned before, we want to concentrate on presenting the results of our TDHF calculations and show the dependency of ω_r on the particle number. In this work, we only investigate the cases $\lambda = 0.1$, 0.3, and 1. Larger values of λ would require to go beyond Hartree-Fock, which demands a very high computational effort. Before we show our results, we start by explaining some important aspects concerning the spectral determination of the breathing frequencies.

A. Spectral analysis

Each of the TDHF frequencies was calculated from a time series that has the length of at least $t_{\text{prop}} = 2500$ (in units Ω^{-1}). Since the resolution in the frequency space is limited by the size of t_{prop}, we applied spline interpolations to the spectra in order to achieve a higher accuracy for the extracted frequency values. Besides, each spectrum was calculated with a Blackman window in order to uncover peaks with small spectral weights.

In Fig. 2, the interesting part of the spectra around the breathing frequencies is shown for rather weak couplings and different particle numbers. The peaks related to ω_r and ω_R can be identified by their dominating spectral weights. The ω_r peak always has the largest amplitude and a smaller frequency than all other peaks. According to the theory, the ω_R peak is to be found around $\omega = 2$. However, one has to deal with two problems when analyzing the spectra. As it can already be surmised in Fig. 2, the HF approximation slightly breaks the universality of the center-of-mass frequency $\omega_R = 2$. With increasing λ the frequency is shifted to higher values and obtains a dependence on the particle number. This can also be seen in Figs. 3–5 for the moderate coupling $\lambda = 1$. The other problem is the occurence of various additional peaks which are uncovered if the propagation time is long enough (see Fig. 3).

The unexpected behavior of the center-of-mass frequency becomes apparent in Fig. 4 for the coupling $\lambda = 1$. One can see that the peaks representing ω_R have a rather strong deviation

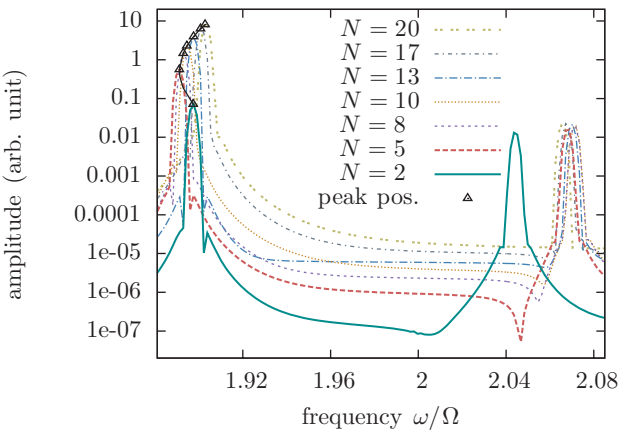

FIG. 4. (Color online) Part of the TDHF monopole spectrum around the breathing frequencies for different particle numbers at the moderate coupling strength $\lambda = 1$. While the relative mode (left peaks) shows a typical behavior, which is also apparent for weak couplings, the center-of-mass mode (right peaks) exhibits too large values and an N dependence that deviates from the exact results. The excitation strength is $\eta = -10^{-3}$.

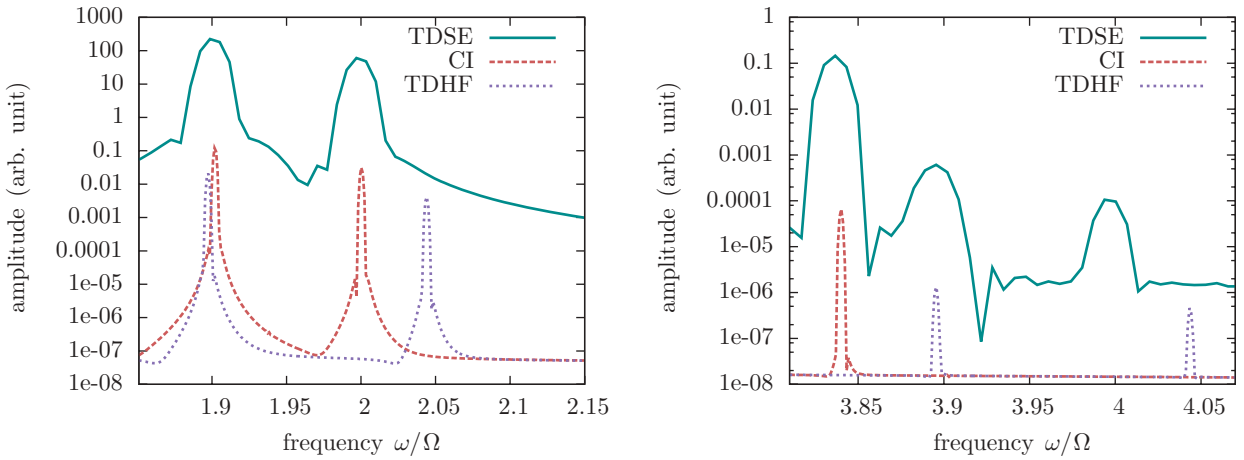

FIG. 5. (Color online) Comparison of the spectra of different methods around the lowest breathing frequencies (left) and their higher harmonics (right) for $N = 2$ and $\lambda = 1$. The TDHF and the CI spectra were obtained for $\eta = -0.0001$ and $t_{\text{prop}} = 6000\ \Omega^{-1}$. While TDHF still shows higher harmonics $2\omega_r$ and $2\omega_R$, they have already vanished for CI. Besides, the leftmost peak in the right image exists only in correlated calculations (CI and TDSE). The CI results show very good agreement with the spectra of the TDSE, which, however, were obtained with $\eta = -1.0$ and $t_{\text{prop}} = 1000\ \Omega^{-1}$, which explains the larger width of the peaks.

from the expected value 2. However, one can convince oneself that, despite the approximate character of TDHF, those peaks represent the center-of-mass mode. As a first possibility, one can observe the behavior of this peak with increasing λ and track the increase of the error. As Fig. 5 shows, if exact solutions are available, one can also use the spectral weights of the peaks as an identifying property. Furthermore, one can check that the spectral weight of the center-of-mass peak decays with the particle number, according to Eq. (28). Since the spectra also show features which result from higher order processes [which in the sense of perturbation theory scale with $\mathcal{O}(\eta^2)$], one can additionally reduce the modulus of the excitation strength η to suppress all frequencies which are not a linear response to the monopole excitation. Hence, a systematic reduction of the excitation strength enables one to identify the relevant peaks by their characteristic linear downscaling.

Especially in the case $\lambda = 1$, it becomes apparent that the excitation must be sufficiently weak. As Fig. 3 shows, an additional peak occurs quite close to $\omega = 2$. This peak could be confused with the center-of-mass peak, but it vanishes if the modulus of η is small enough.

Before we start focusing on the lowest breathing frequency ω_r, we want to recapitulate some properties of the used methods in the exemplary Fig. 5. One can see that the TDHF spectrum always shows higher harmonics of the breathing frequencies ω_r and ω_R. Their spectral weights scale linearly with η. Although higher harmonics also show up in exact methods, their amplitudes are much smaller than those of the TDHF (they already disappeared in the CI curve in the right figure). Of course, in exact methods, processes of higher order are also excited. However, in the figure, they cannot be recognized since the propagation time for the TDSE curve is not long enough, and the CI curve was obtained with a very small modulus of η. Another interesting outcome of the spectrum is an additional peak with frequency $\omega \approx 3.84$, which is missing in the uncorrelated HF approximation. The position of this peak is also predicted by the exact diagonalization method as a process of first order in η.

Having shown how to treat the various features of the spectra, we, from now on, concentrate on the N dependence of the lowest breathing frequency and neglect all higher order processes.

B. Breathing frequencies of finite systems

The TDHF calculations enabled us to obtain the breathing frequencies for up to 20 particles. We found a typical behavior of the breathing frequency ω_r. The analysis of the spectra for the couplings $\lambda = 0.1$, 0.3, and 1 reveals that the N dependency of ω_r is qualitatively the same for all λ. It is characteristic that the frequencies attain a minimum for five particles, before they start steadily growing. This typical behavior is illustrated in Fig. 4. It is qualitatively the same for all weaker couplings. For a complete overview, the explicit values of the breathing frequencies are summarized in the graphs of Fig. 6. For comparison, we also show the TDSE values for $N = 2$ and the CI values for up to eight particles as well as the breathing frequencies obtained with other cutoff parameters. As expected, the TDHF and the CI values are very close [see Fig. 6(a)] for small λ. With increasing λ a constant shift between both results arises. The CI results confirm that the breathing frequency has a minimum with a slightly lower depth and a position of $N = 6$, instead of $N = 5$ particles, in the case of TDHF. Moreover, our analysis of the dependence of the breathing frequency on the cutoff parameter κ indicates that we reached convergence in the range $\kappa^2 = 0.01, \ldots, 0.1$.

Note that the breathing frequency becomes smaller with increasing λ, for $N = \text{const}$. This confirms our previous analysis for $N = 2$, cf. Ref. 14, where we showed that this trend continues to $\omega_r \to \sqrt{3}$ for $\lambda \to \infty$. We expect that this trend persists for $N > 2$ as well, but this is beyond the range where TDHF is reliable.

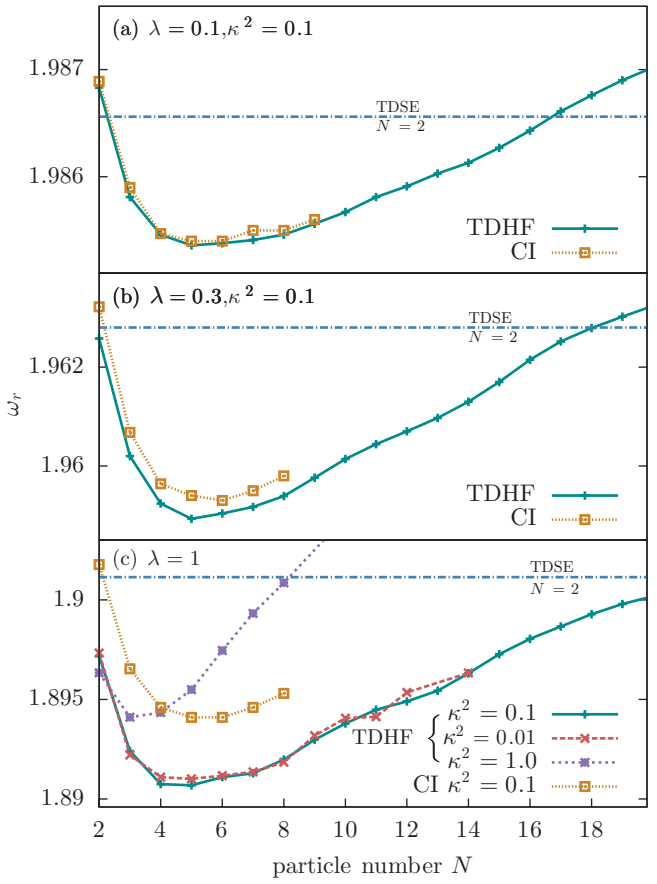

FIG. 6. (Color online) Breathing frequency ω_r vs particle number N for coupling parameters $\lambda = 0.1$, 0.3, and 1 with cutoff parameter $\kappa^2 = 0.1$. For $\lambda = 1$, the frequencies obtained for different κ^2 are also plotted. For comparison, the TDSE frequencies for two particles and the CI results for $N \leqslant 8$ are plotted as well. For $\kappa^2 = 0.1$, the N dependencies are qualitatively the same for all λ.

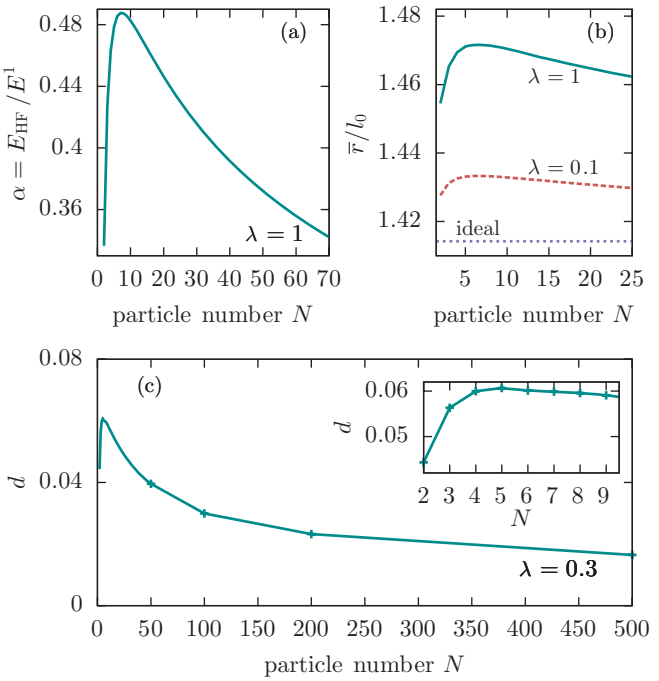

FIG. 7. (Color online) Particle number dependence of various ground-state properties of the interacting system. (a) The effective coupling parameter α, Eq. (39), is nonmonotonic and has a maximum for $N = 7$ particles. (b) The mean particle distance $\bar{r}$, Eq. (40), is nonmonotonic having a maximum for $N = 7$ particles and approaching the ideal limit $\sqrt{2}$, for large N. (c) The point-wise deviation of the density profile from the ideal profile d, Eq. (42), has a maximum for five particles (see inset) and tends to vanish for large particle numbers.

C. Origin of the minimum of $\omega_r(N)$

It is a remarkable and unexpected result that the breathing frequency has a minimum for a small number of particles that appears to be independent of the value of λ. Although this is a result of complex numerical calculations, it is possible to present a physical explanation. Obviously, there are two opposite trends, which influence the value of the breathing frequency. The first decrease of the frequency for slightly more than two particles is due to a growing influence of the interaction energy. For larger particle numbers, however, the frequency approaches the value of the ideal system, where interactions completely vanish.

Since the breathing mode is computed in linear response, this behavior must originate from the *ground-state properties* of the system. This can also be seen from Eq. (35), where the breathing frequency corresponds to a transition between the eigenenergies of the initial Hamiltonian H_0. Although we have no access to the full spectrum of the general N-particle problem for arbitrary couplings, we can validate the observed trends by presenting several characteristic quantities of the ground state. A major advantage is that ground-state properties can be computed for much larger particle numbers than the time dynamics. For the sake of clarity, we re-emphasize that in all following considerations the trap coupling λ is fixed and the particle number will be varied. Further, in all of the following calculations [with the exception of the perturbative ansatz in Eq. (44)] the HF approximation is being used.

1. Role of nonideality effects

As we have seen before, cf. Fig. 6, the breathing frequency monotonically decreases, for N fixed, with the coupling parameter. In other words, the deviation of ω_r from the ideal quantum value 2 appears to be a measure of the role of nonideality effects in the system. Following this argument we may expect that the same relation between ω_r and system nonideality holds also when λ is fixed and N is varied. The results shown in Fig. 6 then suggest that nonideality effects increase for small N and decrease again for large N, reaching a maximum around $N = 5, \ldots, 6$. In the following, we verify this hypothesis by analyzing various quantities that are suitable to characterize the degree of nonideality in a finite system. We then analyze the reasons for the nonmonotonic behavior of the nonideality, in particular, we show that the system becomes ideal in the limit $N \to \infty$.

2. Energy-based nonideality parameter α

An obvious choice of a nonideality parameter is the ratio of interaction energy to the single-particle energy:

$$\alpha(N) = \frac{\langle E_{\rm int}\rangle(N)}{\langle E^1\rangle(N)} = \frac{\langle E_{\rm int}\rangle}{\langle E_{\rm kin}\rangle + \langle E_{\rm pot}\rangle}\,, \tag{39}$$

where, in our calculations, $E_{\rm int}$ is approximated by the Hartree-Fock energy $E_{\rm HF}$. The values of $\alpha(N)$ for up to 70 particles at a fixed value $\lambda = 1$ are shown in Fig. 7(a). Obviously, α first increases, reaches a maximum at $N = 7$ and then converges to zero for large N, indicating that the interaction energy normalized to the single-particle energy vanishes in a macroscopic quantum system.

3. Length-based nonideality parameter $\bar{r}$

As a second indicator we consider the mean interparticle distance $\bar{r}$. The motivation for this is the well-known coupling parameter of the macroscopic homogeneous electron gas r_s (Brueckner parameter) which is the ratio of the mean interparticle distance to the Bohr radius. Since the Bohr radius is a constant, nonideality effects should show up in an N dependence of $\bar{r}$. Identifying the mean interparticle distance of particles in a trap is not trivial since the density profile $n(x)$ is not homogeneous. A reasonable choice is to compute the spatial extension of $n(x)$ and divide it by the number of particles,

$$\bar{r}(N) = \frac{2\sigma(N)}{N}\,. \tag{40}$$

Here, σ is the standard deviation of the particle density $n(x)$ and we use 2σ as an estimator for the spatial extension of the particle cloud in the trap. Obviously, σ is directly related to the expectation value of the potential energy. In particular, for an ideal system, one easily derives

$$\bar{r} = \sqrt{2}\,, \tag{41}$$

as is shown in Appendix A. In Fig. 7(b), the N dependence of $\bar{r}$ is presented for two values of the coupling parameter λ. Again this quantity first increases, reaches a maximum for $N = 7$ and decreases for larger particle numbers, approaching the ideal value.

4. Density profile-based nonideality parameter d

A third indicator of nonideality effects can be derived by comparing the density profile $n(x)$ to the density profile of an ideal system. We consider the quantity

$$d \equiv \frac{1}{N}\int |n(x) - n_{\rm ideal}(x)|\,{\rm d}x\,, \tag{42}$$

where $n_{\rm ideal}$ is the density of the ideal quantum system. We use this quantity to demonstrate the point-wise deviation from the densities in the interacting case from the densities in the noninteracting case. The factor $1/N$ prevents d from diverging and gives it a relative character. (Recall the normalization $\int n(x){\rm d}x = N$.) In order to demonstrate the change in the densities, the normalized densities of the ideal quantum system and the interacting system are plotted for 2 and 30 particles in Fig. 8 for $\lambda = 0.1$. One notices that the largest deviations occur in the trap center ($x = 0$). Finally, the values $d(N)$ for up to 500 particles are shown in Fig. 7(c) for a fixed value $\lambda = 0.3$. Again, one notices that d first increases and tends to vanish for large particle numbers. It reaches a maximum for $N = 5$.

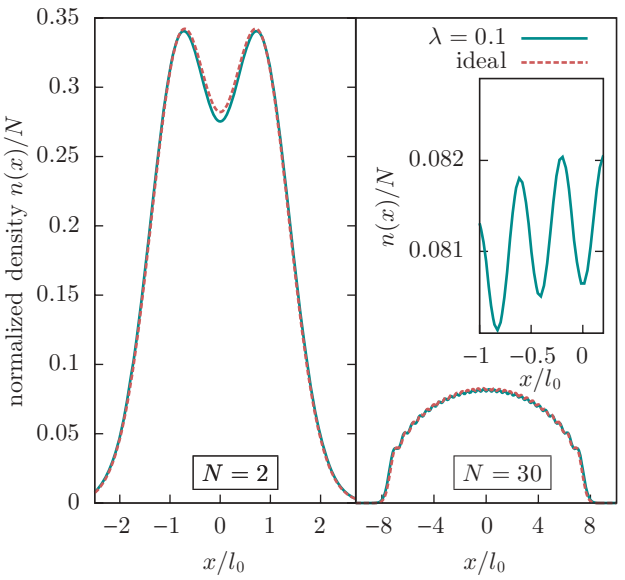

FIG. 8. (Color online) Comparison of the normalized densities of an ideal quantum system and an interacting system ($\lambda = 0.1$) for 2 and 30 particles. The deviation from the ideal system vanishes for large particle numbers.

5. Perturbation theory approach to nonideality

In order to verify that the nonmonotonic N dependence of the nonideality parameters $\alpha, \bar{r}, d$ (and of ω_r) is not an artefact of the used Hartree-Fock approximation, we now perform a calculation in terms of stationary perturbation theory. This has the advantage that many results are available in analytical form. (For the three-dimensional case, see, for example, the work of Garcia.[27])

Let H^0 be the Hamiltonian of the noninteracting (oscillator) system with the assiociated N-particle eigenfunctions $|\Psi_i^0\rangle$. Let further W be the Coulomb operator, then, for sufficiently small couplings ($\lambda < 1$) the energies of the interacting system with the Hamiltonian

$$H = H^0 + \lambda W \tag{43}$$

are well approximated by first-order perturbation theory,

$$E_i = E_i^0 + \lambda \langle \Psi_i^0 | W | \Psi_i^0 \rangle. \tag{44}$$

As in Eq. (39), we define an effective nonideality parameter based on the normalized interaction energy, but now with no restriction to the Hartree-Fock approximation,

$$\tilde{\alpha}(N) = \frac{\langle \Psi_0^0 | W | \Psi_0^0 \rangle(N)}{E_0^0(N)} = \frac{\langle \Psi_0^0 | W | \Psi_0^0 \rangle}{\frac{1}{2}N^2}, \tag{45}$$

for the ideal result, see Appendix A. In Fig. 9, we plot the result for $\tilde{\alpha}(N)$ for up to 55 particles. Obviously, the parameter $\tilde{\alpha}$ shows the same behavior as the Hartree-Fock parameter α, Eq. (39). Interestingly, the parameter $\tilde{\alpha}$ reaches a maximum for $N = 7$ particles. Thus, at least for small couplings, $\lambda < 1$ the observed trends of the nonideality parameter are directly related to the diagonal elements of the interaction matrix W, i.e., to the mean interaction energy in units of the energy of the ideal system. Evidently, for small (large) particle numbers

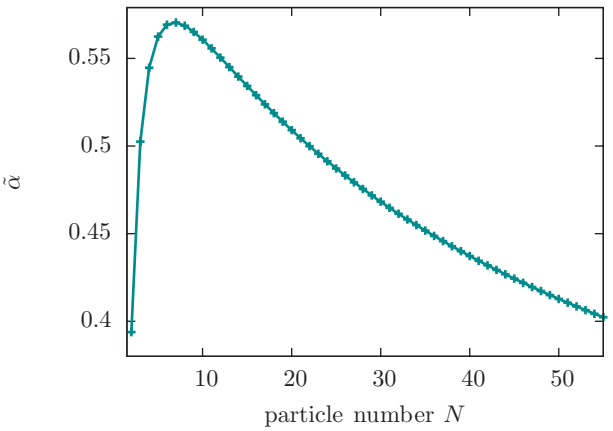

FIG. 9. (Color online) Evolution of the effective nonideality parameter $\tilde{\alpha}$ with increasing particle number. The quantity was obtained in terms of perturbation theory setting $\lambda = 1$. It shows the characteristic maximum for seven particles and a subsequent decrease.

the contribution of this matrix element increases (decreases) faster than the energy of the ideal system.

6. Limits of small and large N

As we have seen, the four nonideality parameters, α, $\bar{r}$, d and $\tilde{\alpha}$ all show the same trend, monotonically increasing up to a maximum at $N = 5$ (for d) or $N = 7$ (for α, $\bar{r}$, and $\tilde{\alpha}$) and then decreasing, eventually approaching the value of the ideal quantum system.

The increase of interaction effects for small particle numbers, $N \geqslant 2$, is easy to understand: the number of pair interactions grows as $N(N-1)/2$. However, it is characteristic for fermions in an oscillator potential that also the energy of the noninteracting system increases proportional to N^2, cf. Eq. (45). Thus there must exist an additional N dependence in the interaction energy resulting from a change of the wave function. On the other hand, the mathematical reason for the decrease of $\tilde{\alpha}$, for large N is that the majority of the particles occupies high energy levels, for which the eigenfunctions are localized increasingly far off the trap center. Therefore the overlap with the Coulomb potential decreases as does the interaction energy. At the same time, the potential energy grows as ($\propto \mathbf{r}_i^2$) when particles are forced to occupy higher orbitals that are localized away from the center, as a consequence of the Pauli principle. These two opposite trends of the potential energy and interaction energy are responsible for the nonmonotonic behavior of the nonideality parameters and of the breathing frequency.

We may attempt an alternative explanation for the vanishing of interaction effects for $N \to \infty$ that is based on the ground-state energy spectrum. At least for small couplings, this behavior can be explained in the single-particle picture of Hartree-Fock orbitals. The interaction causes each particle to have an energy above its corresponding ideal oscillator level. Since this deviation is the largest for the low-lying energy levels, the effect of the interaction becomes smaller when N increases and vanishes in the limit $N \to \infty$. In Fig. 10, this explanation is illustrated for the coupling $\lambda = 0.1$. The figure shows the occupied orbitals and the associated HF energies

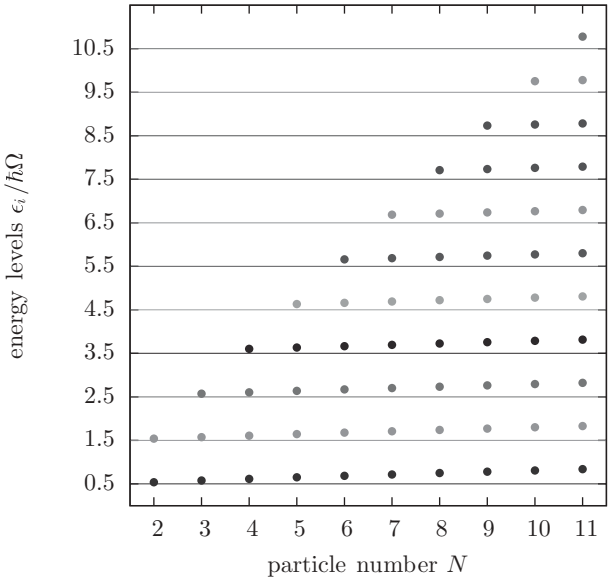

FIG. 10. Occupation of the Hartree-Fock energy levels for different particle numbers for a fixed coupling strength $\lambda = 0.1$. The dots represent the energies of each single particle and the lines the corresponding ideal energy levels $\epsilon_i = i + 1/2$ of the noninteracting system. Adding together the energies of each level for any particle number yields the total energy in the HF approximation. For large particle numbers, the relative deviation from the ideal levels is most dominant in the lower levels.

ϵ_i ($i = 0, \ldots, N-1$), cf. Appendix B, for increasing particle numbers in comparison with the ideal oscillator energies. One can see that for each particle number, the HF energy levels are upshifted by an amount which increases slowly with the particle number. For large particle numbers, the upper energy levels, which mainly contribute to the total energy, have the smallest relative deviation from the ideal levels. Apart from that, the distance between the energy levels also approaches the ideal limit. This can be seen more clearly in Fig. 11, showing that the distances of two neighboring occupied energy levels reach a minimum at low N and then slowly approach the ideal value 1 with increasing N. This has an immediate consequence for the breathing frequency which involves transitions between levels $i \to i + 2$. Due to the Pauli principle, only transitions to unoccupied orbitals are possible, i.e., mostly particles from the levels $i = N - 2$, $N - 1$ can be excited. Since the spacing of these high-lying orbitals converges to the ideal spacing of 2, also the breathing frequency approaches this value.

V. DISCUSSION

This paper was devoted to an analysis of the breathing oscillation—the radial expansion and contraction of particles in a harmonic trap. This mode is one of the most important collective properties, since its frequency allows for a very accurate diagnostics of many system parameters,[14] in particular, the coupling strength. Here, we showed that the breathing frequency ω_r has a nontrivial N dependence if the coupling parameter λ is fixed—it decreases for small N, reaches a minimum for $N = 6$ in CI calculations and $N = 5$ in Hartree-Fock and then increases monotonically again. This

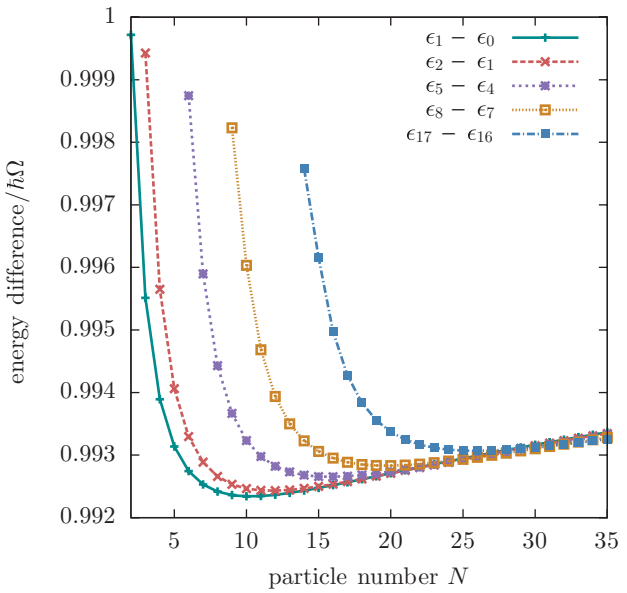

FIG. 11. (Color online) Distances between some selected Hartree-Fock energy levels for $\lambda = 0.1$. Apparently, the spacing of any energy levels decreases to a minimum and then approaches the ideal value 1.

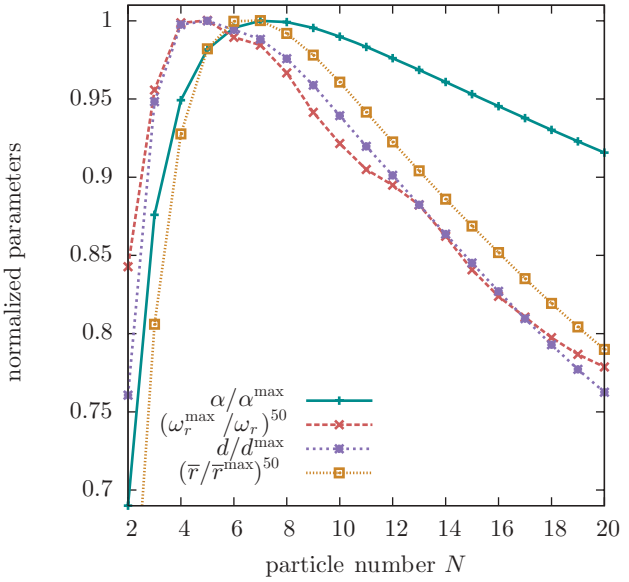

FIG. 12. (Color online) Comparison of the N dependence of several nonideality parameters and of the breathing frequency for $\lambda = 1$. The maxima correspond to the largest nonideality effect, i.e., strongest deviations from the ideal limit.

behavior is in good agreement with the exact results and qualitatively the same for all analyzed coupling strengths, $\lambda = 0.1$, 0.3, and 1. Although for the coupling $\lambda = 1$, the HF approximation is not capable to describe the center-of-mass mode anymore, the recurring characteristic behavior of ω_r supports the trustworthiness of the results in the regime $\lambda \leqslant 1$. We expect that the same nonmonotonic behavior will be observed for arbitrary finite couplings.

The origin of the minimum of ω_r is the competition between two restoring forces: first, the Coulomb repulsion between the particles, which is strongest for $\lambda \to \infty$ (point charges) and which favors $\omega_r = \sqrt{3}$. Second, the kinetic energy of a quantum system that is maximal for $\lambda = 0$ and favors the value $\omega_r = 2$. As our ground-state analysis shows, the minimum of ω_r can be related to the ratio of the expectation values of those energies. Indeed, the associated nonideality parameters α (in Hartree-Fock) and $\tilde{\alpha}$ (in perturbation theory) show exactly the same nonmonotonic behavior reaching a maximum at the slightly higher particle number $N = 7$. We further studied two other quantities that are suitable measures of the degree of nonideality: the mean interparticle distance $\bar{r}$ (that takes over the role of the Brueckner parameter r_s of a homogeneous macroscopic electron gas) and the parameter d that characterizes the deviation of the density profile $n(x)$ from the ideal one. These parameters are also nonmonotonic functions of N with a maximum at $N = 7$ (for $\bar{r}$) and $N = 5$ (for d), respectively.

To better compare the dependence of the different nonideality parameters and the breathing frequency on the particle number, we plot them together in Fig. 12 for the coupling $\lambda = 1$. All quantities are normalized to their maximum value (α, d, $\bar{r}$) or to their minimum values (ω_r), respectively. For better comparison, ω_r and $\bar{r}$ are rescaled (by raising them to the power 50). There is remarkable agreement of the overall trend of these quantities as a function of the particle number. Although there is a slight discrepancy with respect to the exact position of the extremum there is no question that the explanation of the minimum of ω_r in terms of largest nonideality is appropriate. Even though our result was obtained in Hartree-Fock approximation, the CI results confirm that this nonmonotonic behavior is not a property of the approximation but a physical effect. The CI data suggest that the minimum of ω_r is reached for $N = 6$ in a one-dimensional system.

While our time-dependent HF simulations allowed us to determine the frequencies for up to 20 particles at weak and moderate coupling ($\lambda \leqslant 1$), we found strong hints that the increase of ω_r will continue for $N > 20$, and for $N \to \infty$, the breathing frequency will converge to the frequency $\omega = 2$ of an ideal quantum system, for arbitrary fixed λ. On the other hand, if the particle number N is fixed and the limit $\lambda \to \infty$ is taken, the system always approaches a classical system[16,18] that has the universal frequency $\sqrt{3}$, for arbitrary fixed N. This behavior, which is also known as Wigner crystallization, can be forced by decreasing the trap frequency, i.e., $\Omega \to 0$. The reason for such a classical behavior is the strong separation of the wave function.

The appearance of the two different limiting frequencies is only an apparent contradiction, as the result depends on the way the limits $\lambda \to \infty$ and $N \to \infty$ are taken. To demonstrate the scaling of interaction effects with the particle number, we define a quantum degeneracy parameter for particles in a harmonic trap as

$$\chi = \frac{l_0}{\bar{r}} \,. \tag{46}$$

This quantity is the ratio of the extension of the wave function, which is estimated by l_0 (the extension of the ideal ground-state wave function), and the average distance between the particles, $\bar{r}$. Although the exact definition of $\bar{r}$ always involves a certain arbitrariness, this parameter is useful since it allows

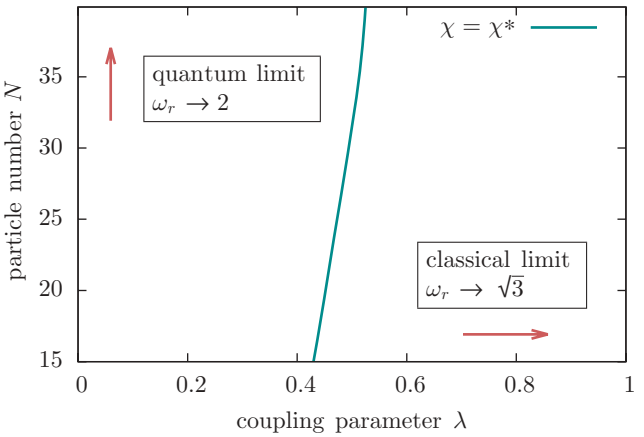

FIG. 13. (Color online) Illustration of the two limiting values of the breathing frequency ω_r for large N and λ (the direction of the limit is indicated by arrows). The line indicates a constant quantum degeneracy parameter $\chi = \chi* \approx 0.68$, separating the quantum and the classical regime. The data are obtained from stationary HF calculations.

for a qualitative separation of the classical ($\chi \to 0$) and the quantum ($\chi \to 1/\sqrt{2}$) regimes. This is shown schematically in Fig. 13. In the area above (below), the line $\chi = \chi* = \text{const}$, quantum (classical) behavior is dominant. While our present HF results limit us to moderate λ and particle numbers, it remains a subject of future work to extend the curve to larger particle numbers and coupling strengths where we expect that this trend will be confirmed. Larger couplings can be accessed, e.g., in quantum kinetic simulations including correlations, at least on the level of the Born approximation, e.g., Ref. 28. Another promising route is to use a stationary approach based on *ab initio* quantum Monte Carlo data.[29] Finally, it will be interesting to extend the present analysis to higher dimensions or/and other interactions (e.g., dipole interaction) as well as to bosonic systems.

ACKNOWLEDGMENTS

This work is supported by the Deutsche Forschungsgemeinschaft via project BO1366-9 and by grant SPH006 for computer time at the HLRN.

APPENDIX A: PROPERTIES OF N NONINTERACTING FERMIONS IN A HARMONIC TRAP

The ideal quantum system is a standard textbook problem. We briefly recall some results that have been used in the main text. In the noninteracting case, the problem reduces to that of the single-particle harmonic oscillator

$$\left(-\frac{1}{2}\nabla^2 + \frac{1}{2}\mathbf{r}^2\right)\phi_i(\mathbf{r}) = \epsilon_i\phi_i(\mathbf{r})\,. \tag{A1}$$

The eigenfunctions ϕ_i are expressed in terms of the Hermite polynomials with the associated eigenvalues $\epsilon_i = i + d/2$. If the N-particle system is spin polarized, the Pauli principle forces each of the N particles to occupy one of those energy levels, starting from the bottom (ground state). In the one-dimensional case, the total energy of the ground state is then given by

$$E_0 = \sum_{i=0}^{N-1}\left(i + \frac{1}{2}\right) = \frac{1}{2}N^2\,, \tag{A2}$$

where the potential energy E_{pot} equals $E_0/2$, for arbitrary N. The standard deviation of the one-particle density (width) reads

$$\sigma = \left[\int n(x)(x-\overline{x})^2\,\mathrm{d}x\right]^{1/2}\,. \tag{A3}$$

As the average value $\overline{x}$ is zero, one finds

$$\sigma = \left[\int n(x)x^2\,\mathrm{d}x\right]^{1/2} = [2E_{\text{pot}}]^{1/2} = \frac{1}{\sqrt{2}}N. \tag{A4}$$

APPENDIX B: CALCULATION OF THE HARTREE-FOCK GROUND-STATE ENERGIES

We briefly explain some details of the self-consistent Hartree-Fock method for the calculation of the HF orbital energies from Fig. 10. Let

$$h(x) = -\frac{1}{2}\nabla_x^2 + \frac{1}{2}x^2 \tag{B1}$$

be the single-particle Hamiltonian without interactions. Including the Hartree-Fock potential, the system is described by the effective Hamiltonian

$$H^{\text{eff}} = \int \mathrm{d}x \int \mathrm{d}x'\psi^\dagger(x)[h(x)\delta(x-x') + \lambda\Sigma^{\text{HF}}(x,x')]\psi(x'), \tag{B2}$$

where $\psi^\dagger(x)$ and $\psi(x')$ are the creation and annihilation operators and the Hartree-Fock self-energy is given by

$$\Sigma^{\text{HF}}(x,x') = \int \mathrm{d}\overline{x}\left[F^1(\overline{x},\overline{x})\frac{1}{|\overline{x}-x|}\delta(x-x') - F^1(x',x)\frac{1}{|x'-x|}\right]. \tag{B3}$$

The density matrix can be determined in an iterative scheme, using the Roothaan-Hall equations.[24] Finally, the total energy can be calculated by

$$E_{\text{tot}} = \frac{1}{2}\sum_{i=0}^{N-1}E_i + \frac{1}{2}\text{Tr}(h^0F^1), \tag{B4}$$

where the E_k are the N lowest eigenvalues of H^{eff}. In this expression, the double counting of the Hartree-Fock potential energy in the orbitals E_i is compensated by the addition of the non-interacting energy $\text{Tr}(h^0F^1)$ and weighting both terms with $1/2$. If H^{eff} is diagonalized under the unitary transformation $U^\dagger H^{\text{eff}}U$, the density matrix

$$\tilde{F}^1 = U^\dagger F^1 U \tag{B5}$$

is also diagonal with

$$(\tilde{F}^1)_{ik} = \begin{cases} 1 & \text{for } i = k, \quad i \in \{0\ldots N-1\}\,, \\ 0 & \text{otherwise,} \end{cases} \tag{B6}$$

i.e., only the first N entries on the diagonal are occupied with a 1 and all other entries are zero. Defining

$$\tilde{h}^0 = U^\dagger h^0 U \ , \tag{B7}$$

one can write

$$E_{\rm tot} = \sum_{i=0}^{N-1} \epsilon_i \tag{B8}$$

with

$$\epsilon_i \equiv \frac{1}{2} E_i + \frac{1}{2} (\tilde{h}^0)_{ii} \ . \tag{B9}$$

Hence, each Hartree-Fock orbital contributes to the total energy with an associated eigenvalue of the effective Hamiltonian (usually denoted as spin orbital energy) and another compensating energy from the noninteracting system.

*abraham@theo-physik.uni-kiel.de

[1] F. Baletto and R. Ferrando, Rev. Mod. Phys. **77**, 371 (2005).

[2] A. V. Filinov, M. Bonitz, and Y. E. Lozovik, Phys. Rev. Lett. **86**, 3851 (2001).

[3] A. V. Filinov, Y. E. Lozovik, and M. Bonitz, Phys. Status Solidi B **221**, 231 (2000).

[4] S. M. Reimann and M. Manninen, Rev. Mod. Phys. **74**, 1283 (2002).

[5] I. Bloch, Nat. Phys. **1**, 23 (2005).

[6] S. Giorgini, L. P. Pitaevskii, and S. Stringari, Rev. Mod. Phys. **80**, 1215 (2008).

[7] A. Görlitz, J. M. Vogels, A. E. Leanhardt, C. Raman, T. L. Gustavson, J. R. Abo-Shaeer, A. P. Chikkatur, S. Gupta, S. Inouye, T. Rosenband, and W. Ketterle, Phys. Rev. Lett. **87**, 130402 (2001).

[8] C. Menotti and S. Stringari, Phys. Rev. A **66**, 043610 (2002).

[9] H. Moritz, T. Stöferle, M. Köhl, and T. Esslinger, Phys. Rev. Lett. **91**, 250402 (2003).

[10] P. Pedri, S. De Palo, E. Orignac, R. Citro, and M. L. Chiofalo, Phys. Rev. A **77**, 015601 (2008).

[11] I. Bloch, J. Dalibard, and W. Zwerger, Rev. Mod. Phys. **80**, 885 (2008).

[12] A. Filinov, J. Böning, M. Bonitz, and Y. Lozovik, Phys. Rev. B **77**, 214527 (2008).

[13] J. Böning, A. Filinov, and M. Bonitz, Phys. Rev. B **84**, 075130 (2011).

[14] S. Bauch, K. Balzer, C. Henning, and M. Bonitz, Phys. Rev. B **80**, 054515 (2009).

[15] S. Bauch, D. Hochstuhl, K. Balzer, and M. Bonitz, J. Phys. Conf. Ser. **220**, 012013 (2010).

[16] B. Partoens and F. M. Peeters, J. Phys.: Condens. Matter **9**, 5383 (1997).

[17] D. H. E. Dubin and J. P. Schiffer, Phys. Rev. E **53**, 5249 (1996).

[18] C. Henning, K. Fujioka, P. Ludwig, A. Piel, A. Melzer, and M. Bonitz, Phys. Rev. Lett. **101**, 045002 (2008).

[19] M. Bonitz, *Quantum Kinetic Theory* (B.G. Teubner, Stuttgart/Leipzig, 1998).

[20] N. N. Bogolyubov, *Problems of Dynamical Theory in Statistical Physics* (Gostekhisdat (russ), Moscow, 1946).

[21] N. Bogolyubov, *Studies in statistical mechanics* (North-Holland, Amsterdam, 1962), Vol. 1.

[22] Yu. L. Klimontovich, D. Kremp, and W. D. Kraeft, *Kinetic Theory for Chemically Reacting Gases and Partially Ionized Plasmas*, in Advances in Chemical Physics, edited by I. Prigogine and S. A. Rice (John Wiley & Sons, Inc., Hoboken, NJ, 2007), Vol. 68, pp. 175–253.

[23] D. B. Boercker and J. W. Dufty, Ann. Phys. **119**, 43 (1979).

[24] C. C. J. Roothaan, Rev. Mod. Phys. **23**, 69 (1951).

[25] T. N. Rescigno and C. W. McCurdy, Phys. Rev. A **62**, 032706 (2000).

[26] K. Balzer, S. Bauch, and M. Bonitz, Phys. Rev. A **81**, 022510 (2010).

[27] J. Z. Garcia, J. Math. Phys. **46**, 122104 (2005).

[28] K. Balzer, M. Bonitz, R. van Leeuwen, N. E. Dahlen, and A. Stan, Phys. Rev. B **79**, 245306 (2009); K. Balzer and M. Bonitz, J. Phys. A **42**, 214020 (2009); K. Balzer, S. Hermanns, and M. Bonitz, Europhys. Lett. **98**, 67002 (2012).

[29] T. Schoof, M. Bonitz, A. Filinov, D. Hochstuhl, and J. W. Dufty, Contrib. Plasma Phys. **51**, 687 (2011).